FIG. 1

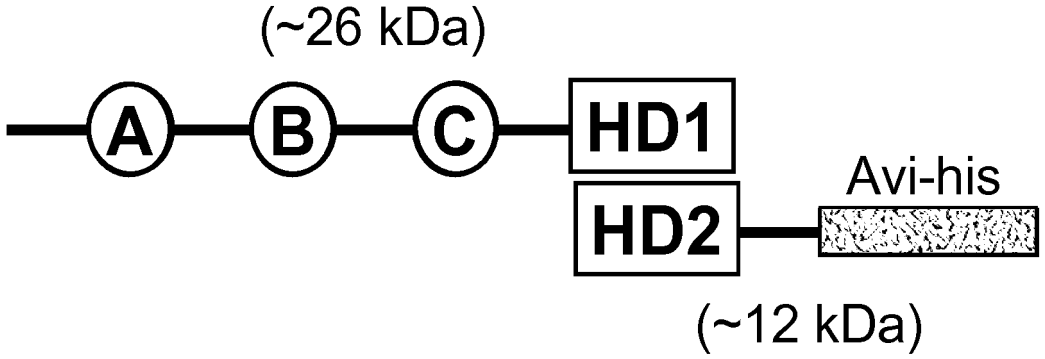
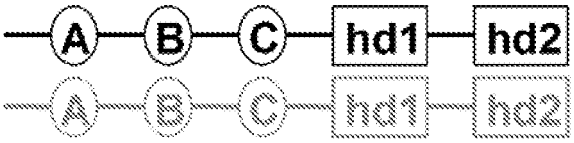
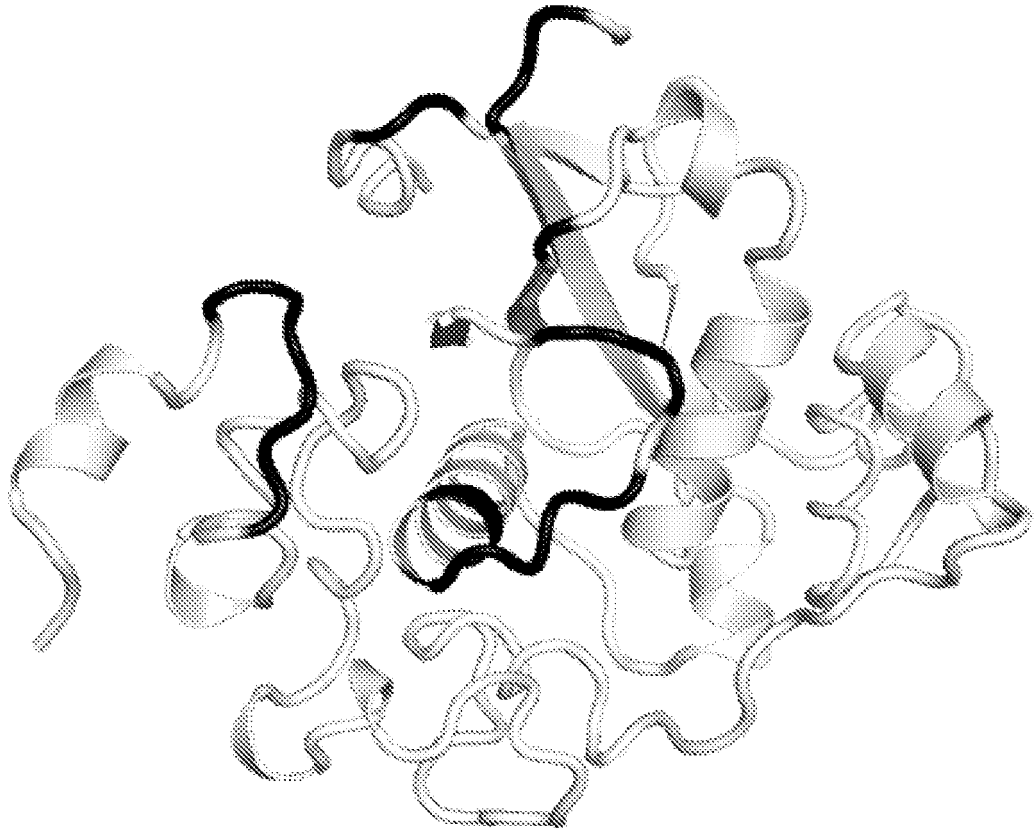


FIG. 2



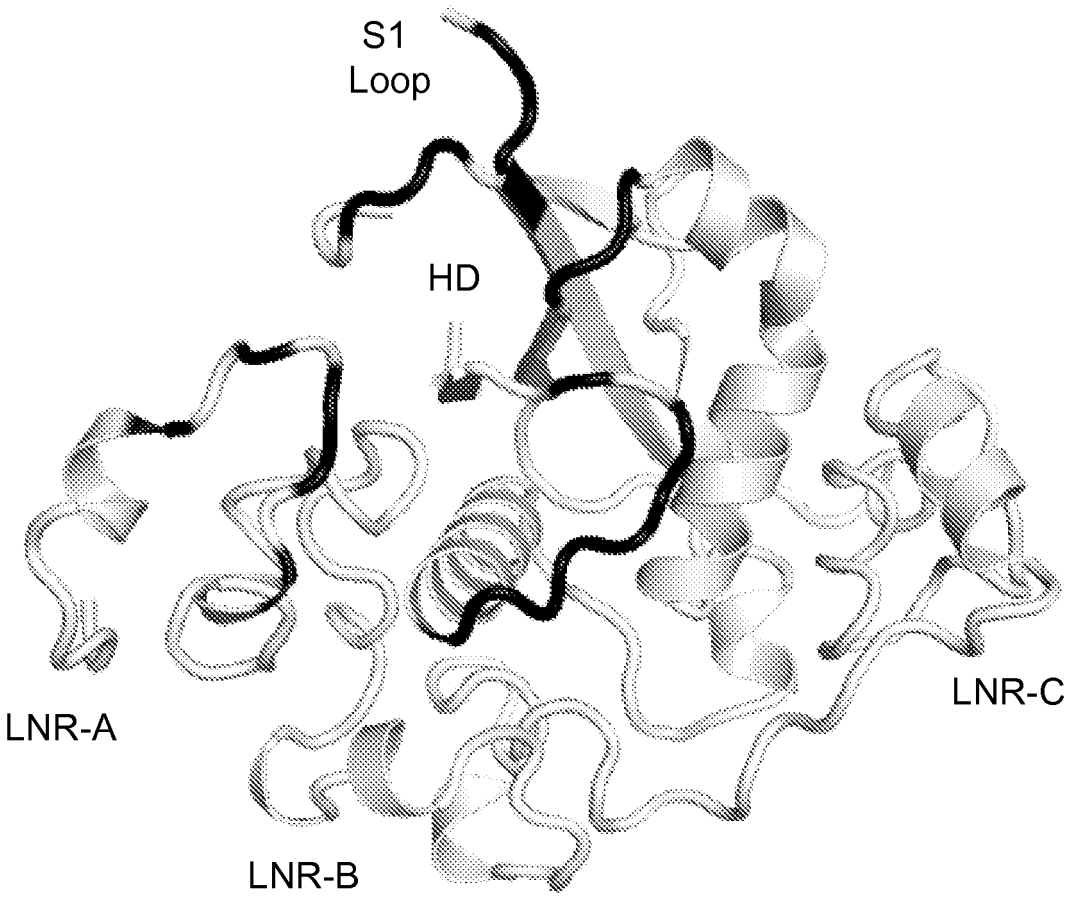
Anti Notch1:	Rat 351-mIgG1	Rat 438-mIgG1	A2
A B C hd1 hd2	57	51	75
A B C hd1 hd2	40	1	1
A B C hd1 hd2	78	6	2
A B C hd1 hd2	56	2	6
A B C hd1 hd2	20	15	6
A B C hd1 hd2	55	47	70
A B C hd1 hd2	34	29	50
A B C hd1 hd2	0	0	0
A B C hd1 hd2	60	53	83

FIG. 3



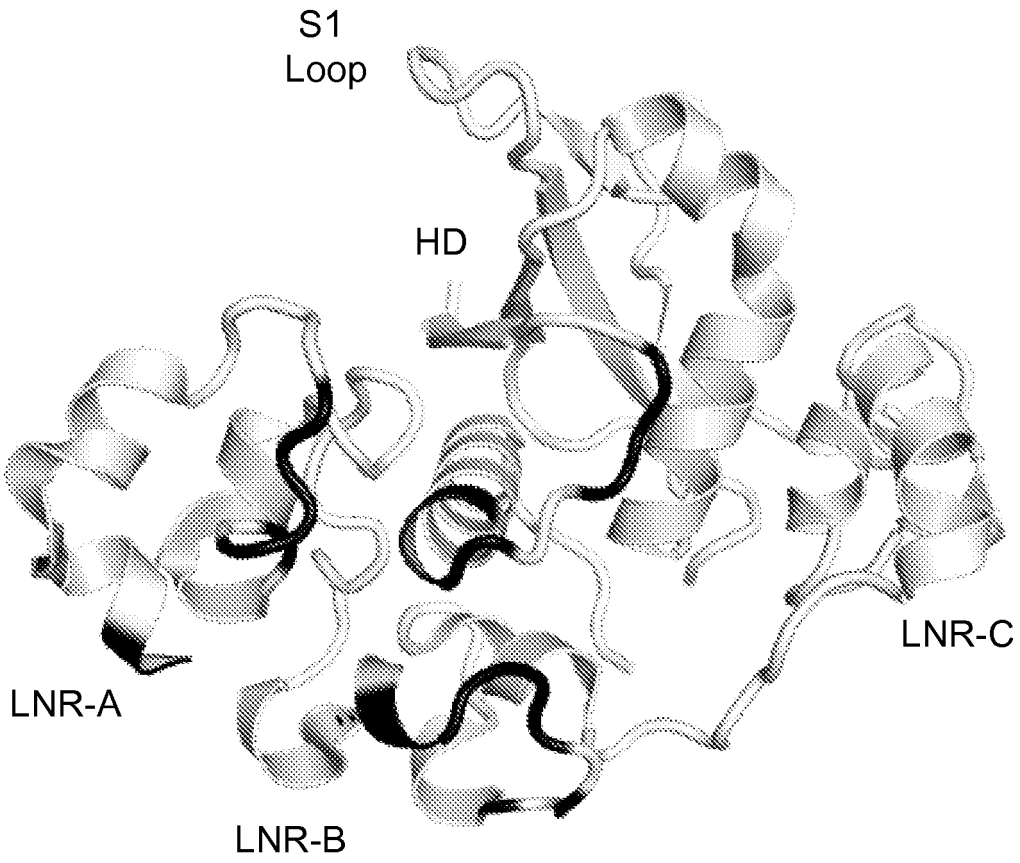
Rat 438 epitope on human Notch1 NRR

FIG. 4



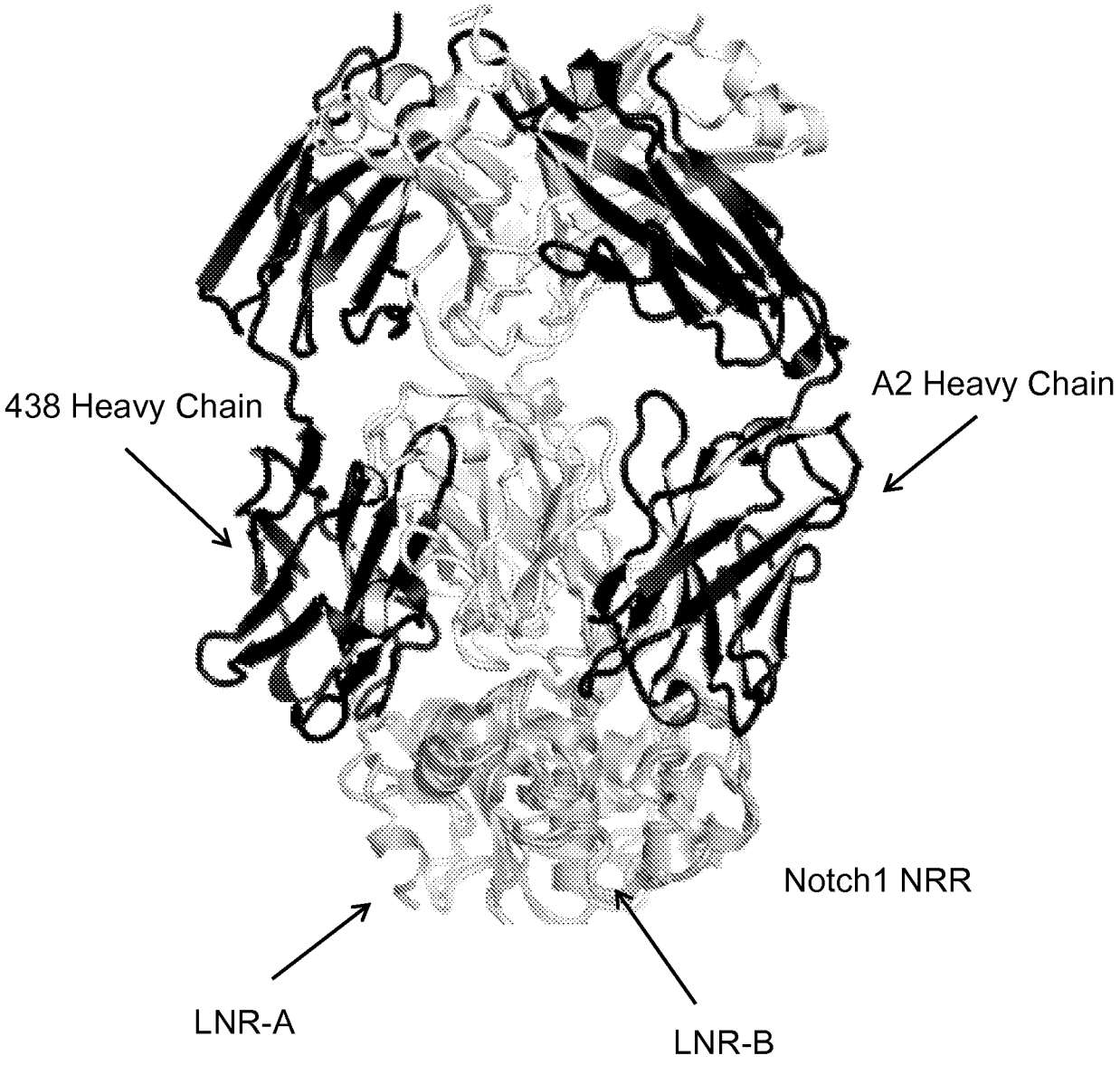
Rat 351 epitope on human Notch1 NRR

FIG. 5



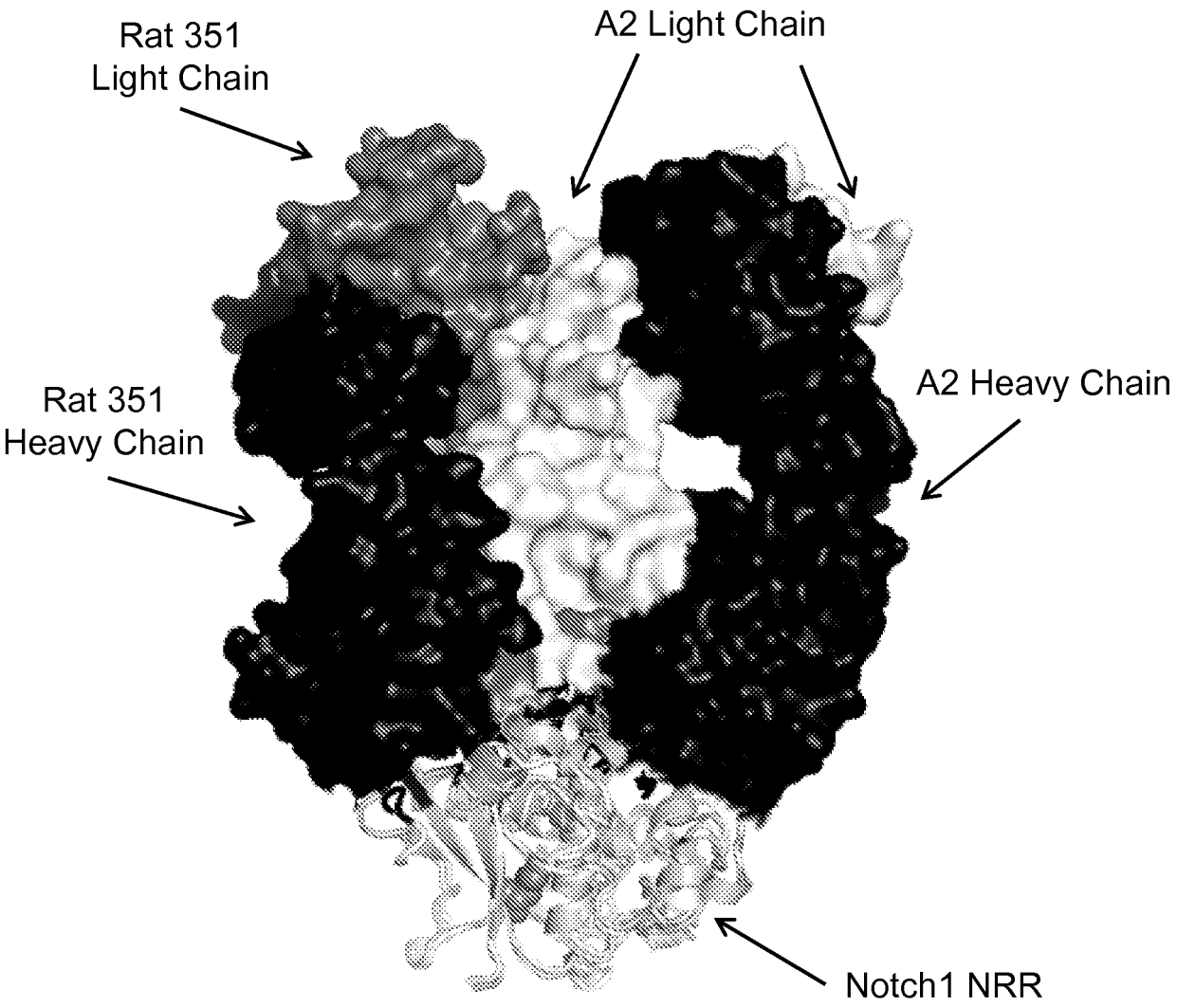
A2 epitope on human Notch1 NRR

FIG. 6



Superposition of the structures of human Notch1 NRR bound to rat 438 and A2

FIG. 7



Superposition of the structures of human Notch1 NRR bound to rat 351 and A2

FIG. 8

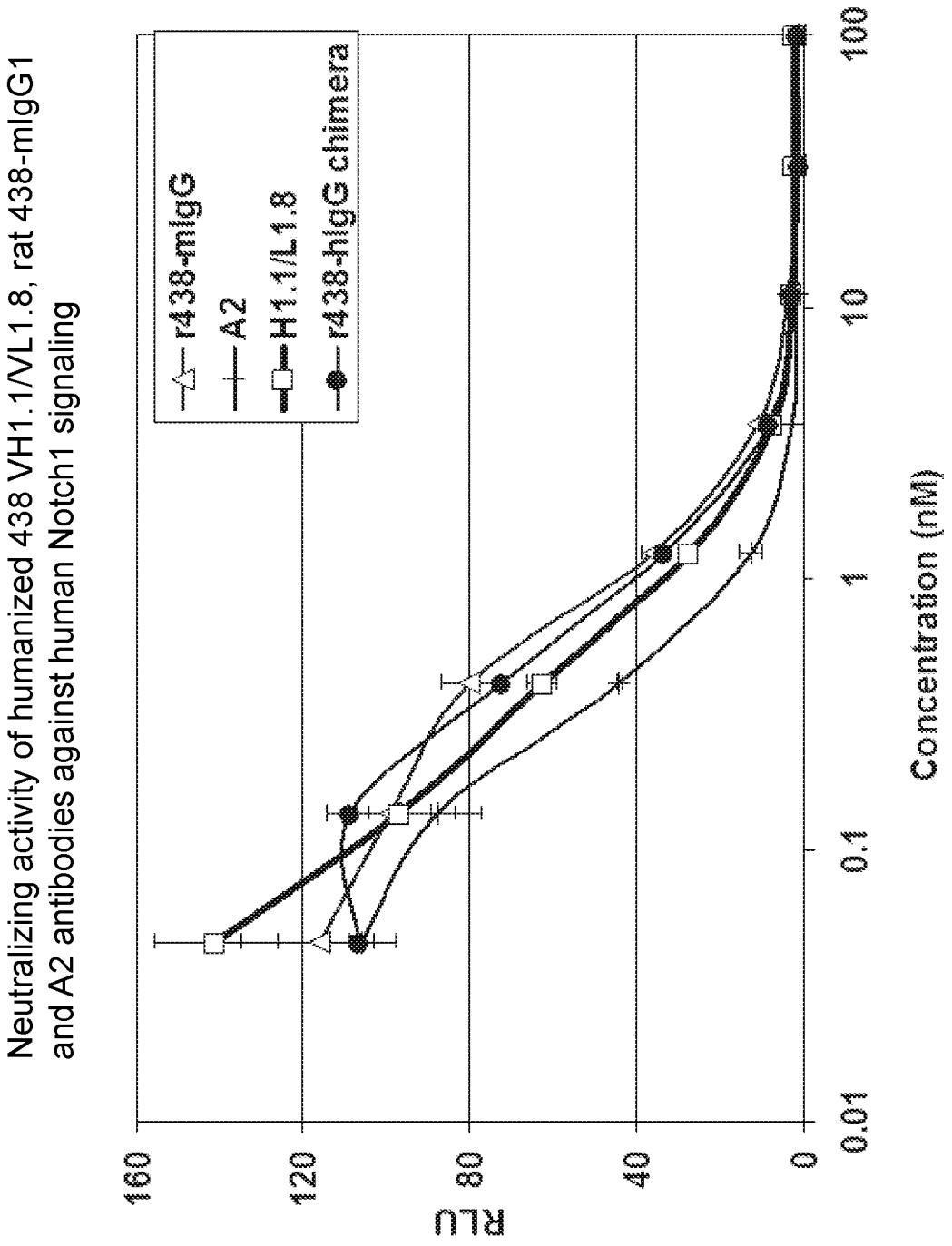

Neutralizing activity of humanized 438 VH1.1/VL1.8, rat 438-mIgG1 and A2 antibodies against human Notch1 signaling
r438-mIgG
A2
H1.1/L1.8
r438-hIgG chimera
RLU
160
120
80
40
0
0.01
0.1
1
10
100
Concentration (nM)

FIG. 9

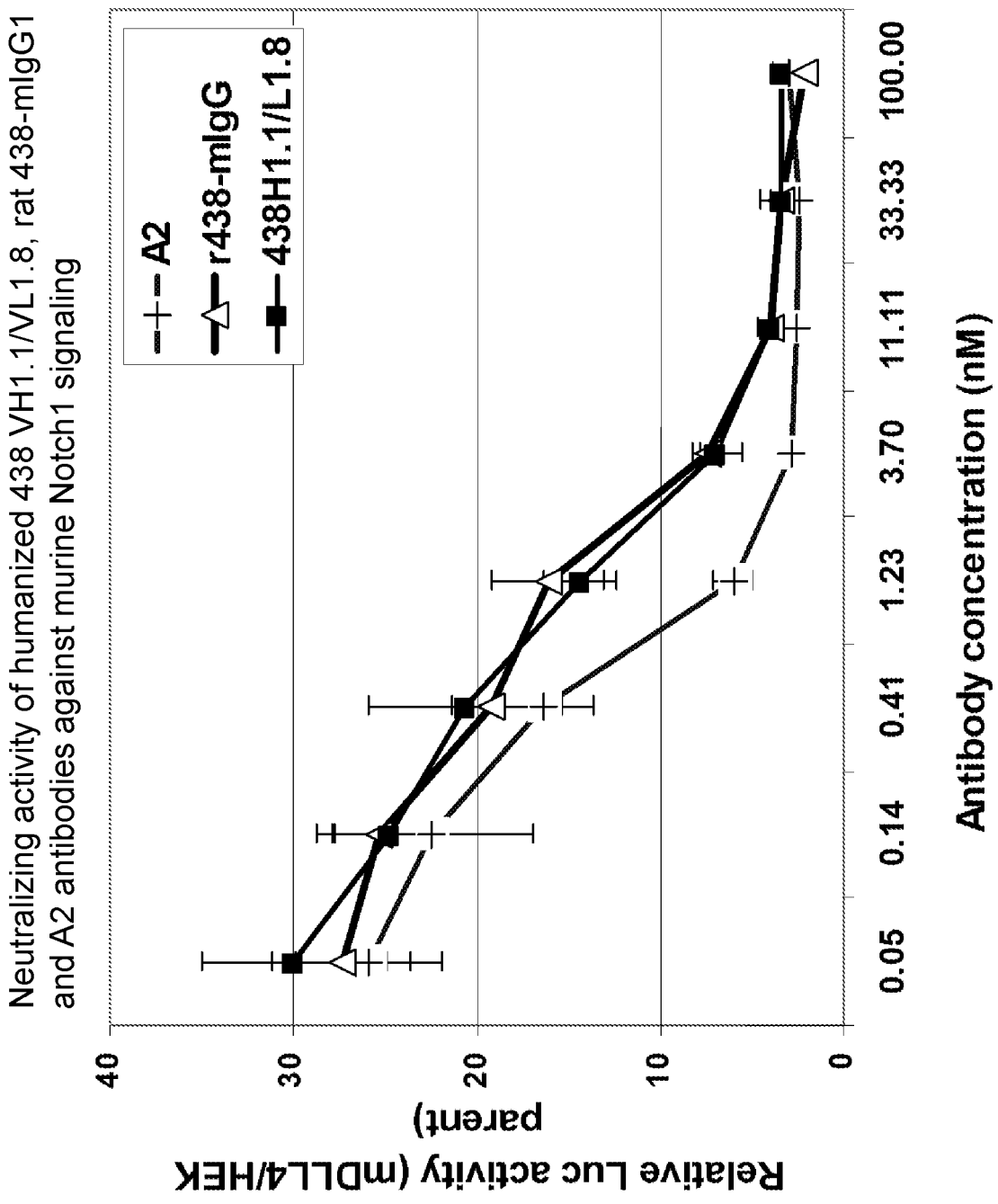
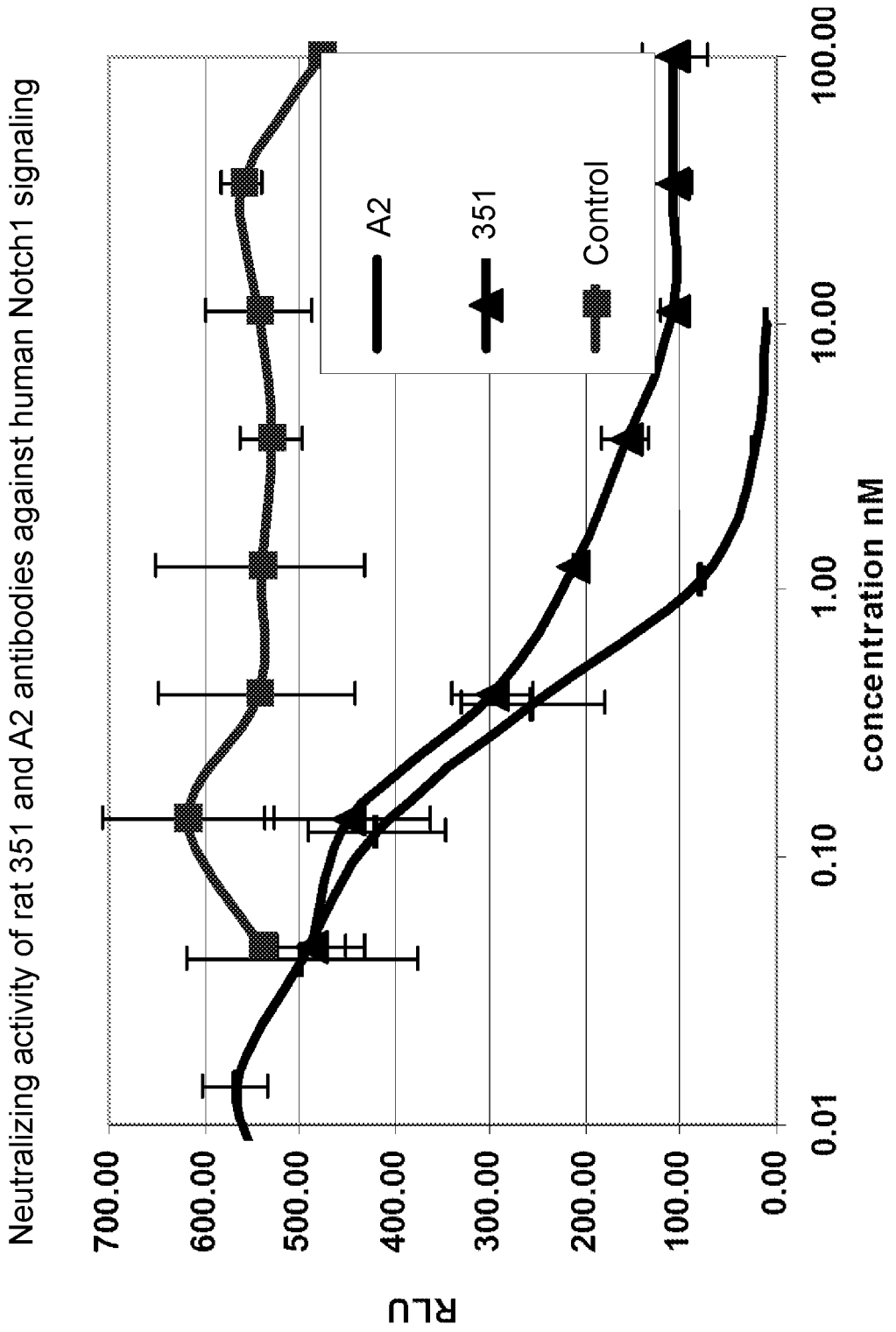

Neutralizing activity of humanized 438 VH1.1/VL1.8, rat 438-mIgG1 and A2 antibodies against murine Notch1 signaling
A2
r438-mIgG
438H1.1/L1.8
Relative Luc activity (mDLL4/HEK parent)
0
10
20
30
40
0.05
0.14
0.41
1.23
3.70
11.11
33.33
100.00
Antibody concentration (nM)

FIG. 10


Neutralizing activity of rat 351 and A2 antibodies against human Notch1 signaling
RLU
700.00
600.00
500.00
400.00
300.00
200.00
100.00
0.00
0.01
0.10
1.00
10.00
100.00
concentration nM
A2
351
Control

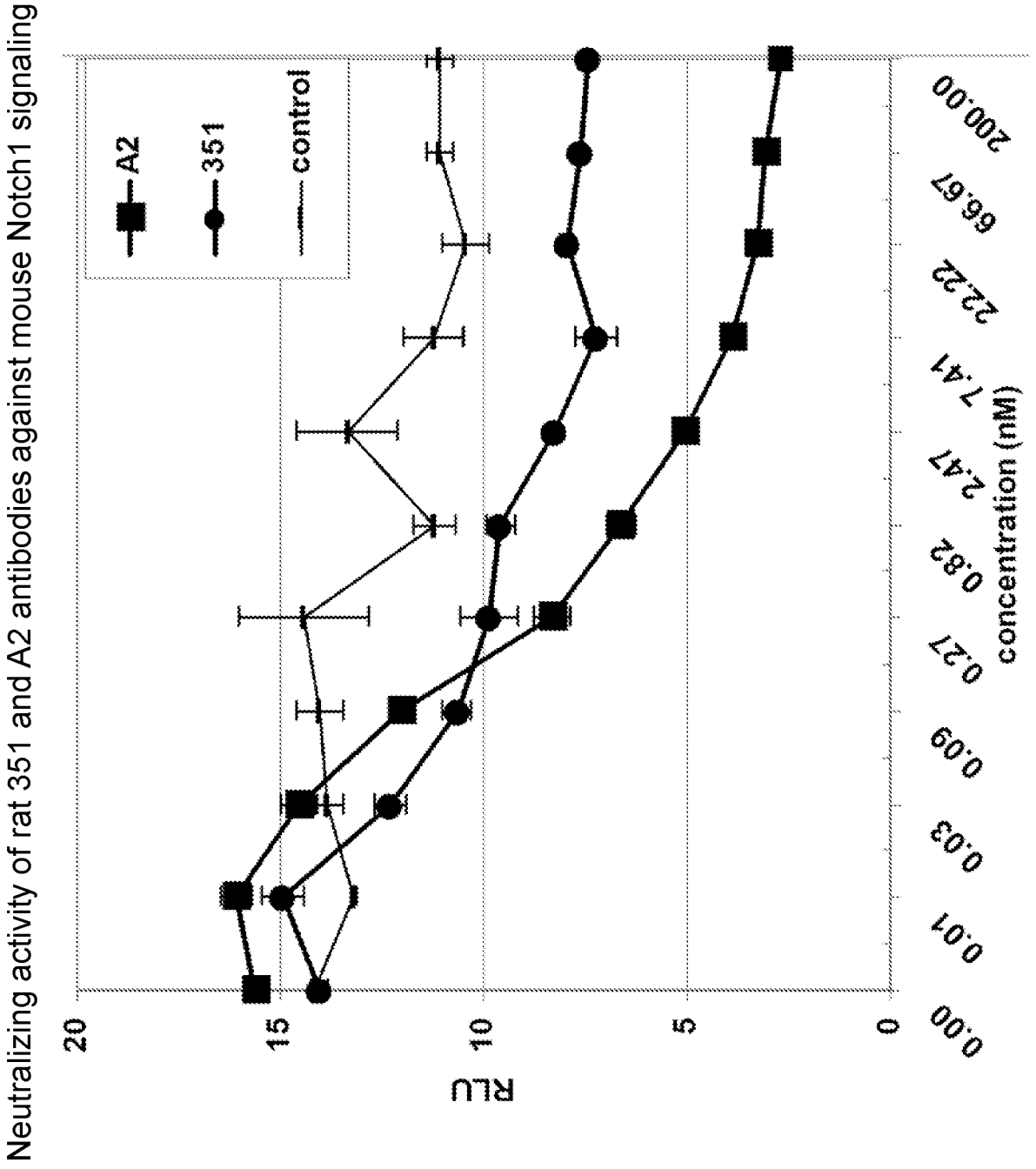

Neutralizing activity of rat 351 and A2 antibodies against mouse Notch1 signaling
A2
351
control
RLU
20
15
10
5
0
0.00
0.01
0.03
0.09
0.27
0.82
2.47
7.41
22.22
66.67
200.00
concentration (nM)

FIG. 11

FIG. 12

Neutralizing activity of humanized 351 variants, rat 351-mIgG1 and A2 antibodies against human Notch1 signaling

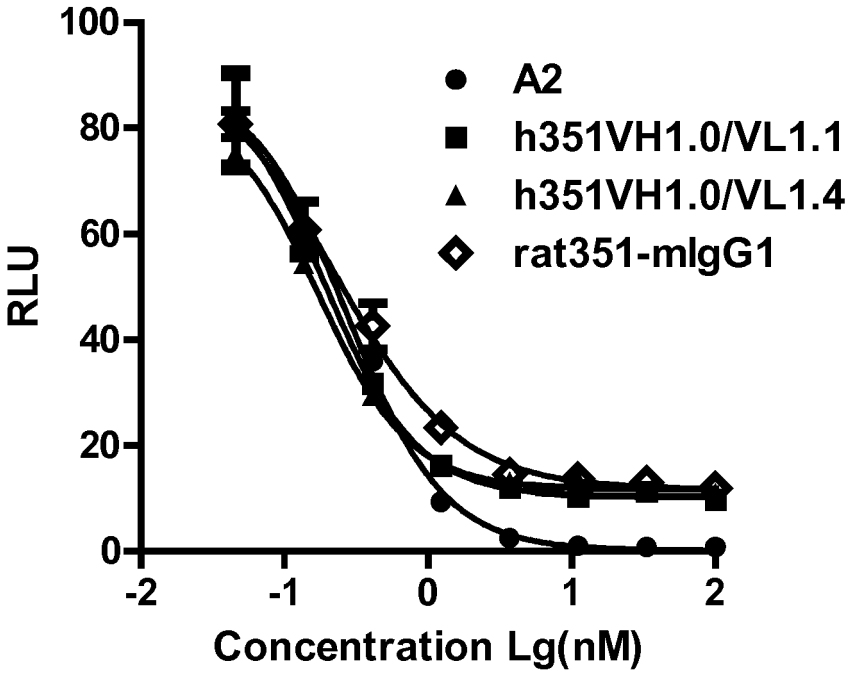


FIG. 13

Neutralizing activity of humanized 351 variants, rat 351-mIgG1 and A2 antibodies against human Notch1 signaling

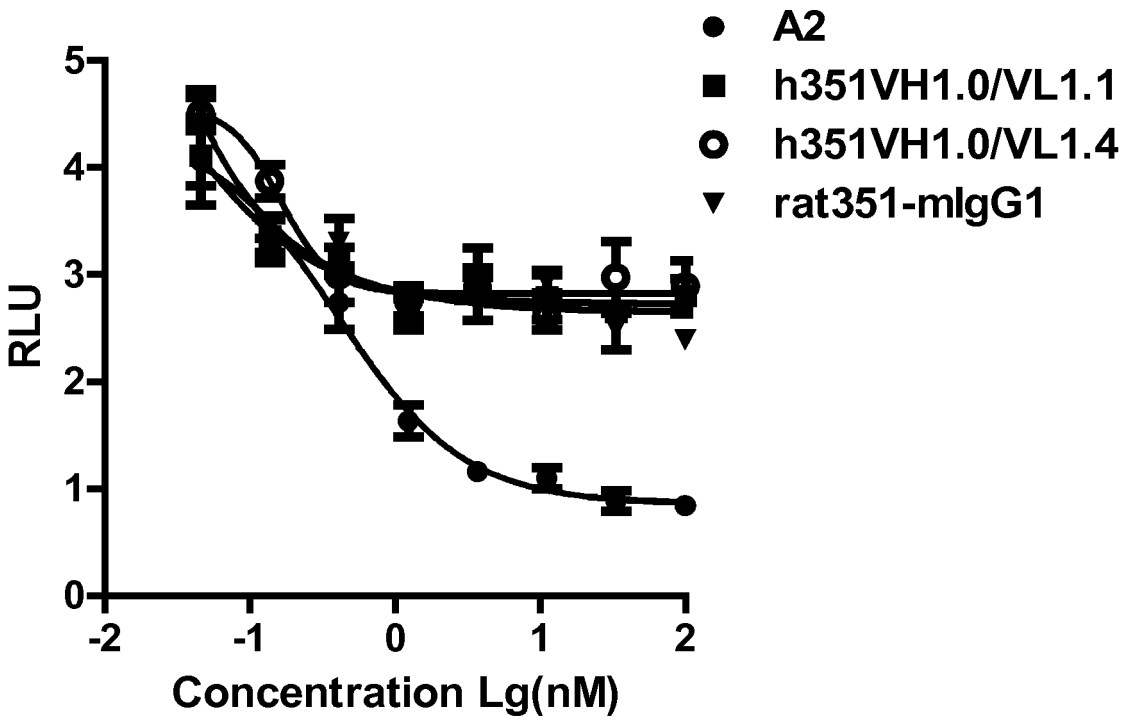


FIG. 14A

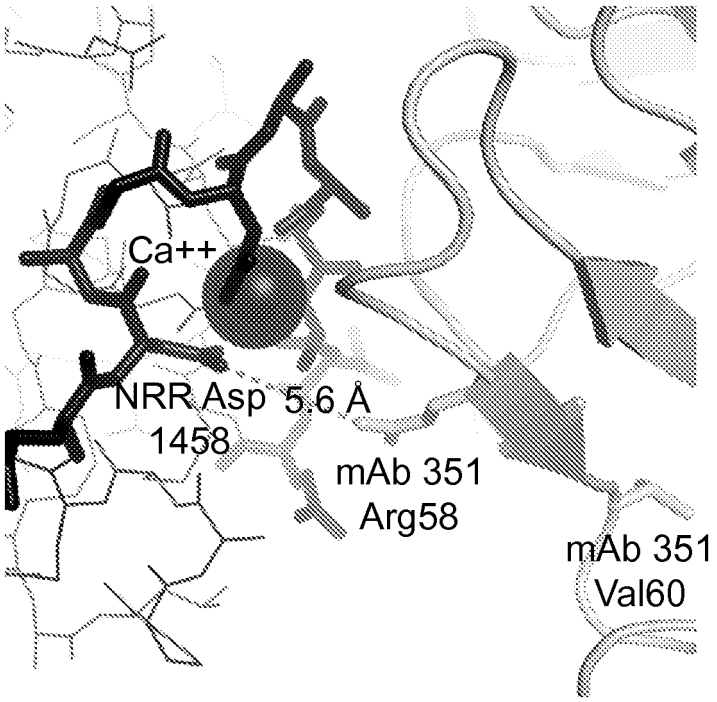


FIG. 14B

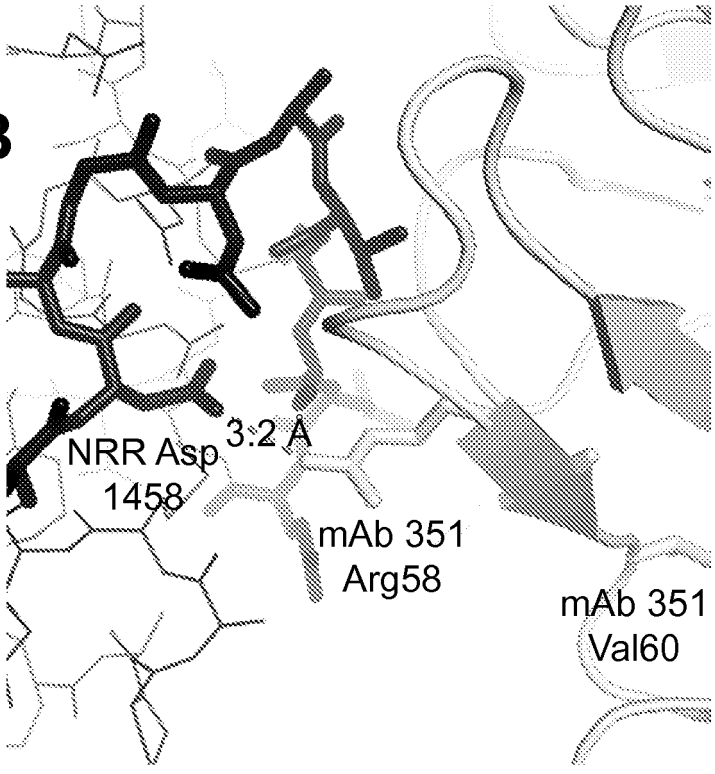


FIG. 15

Neutralization activity of rat 351, mutant rat 351 and A2 in co-culture reporter gene assays

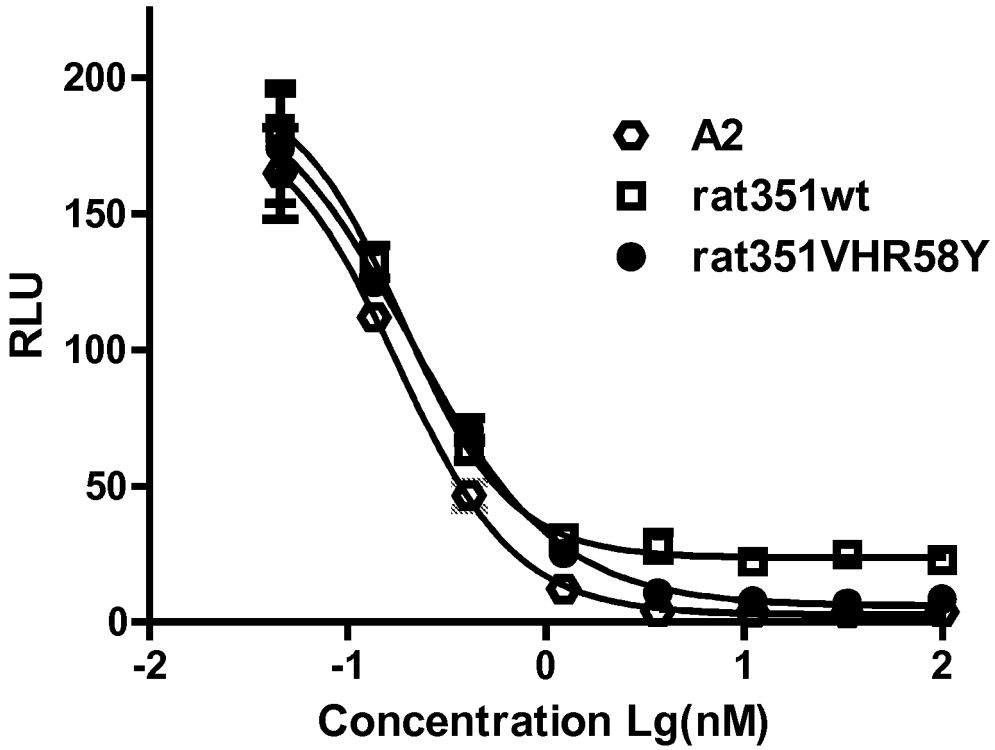
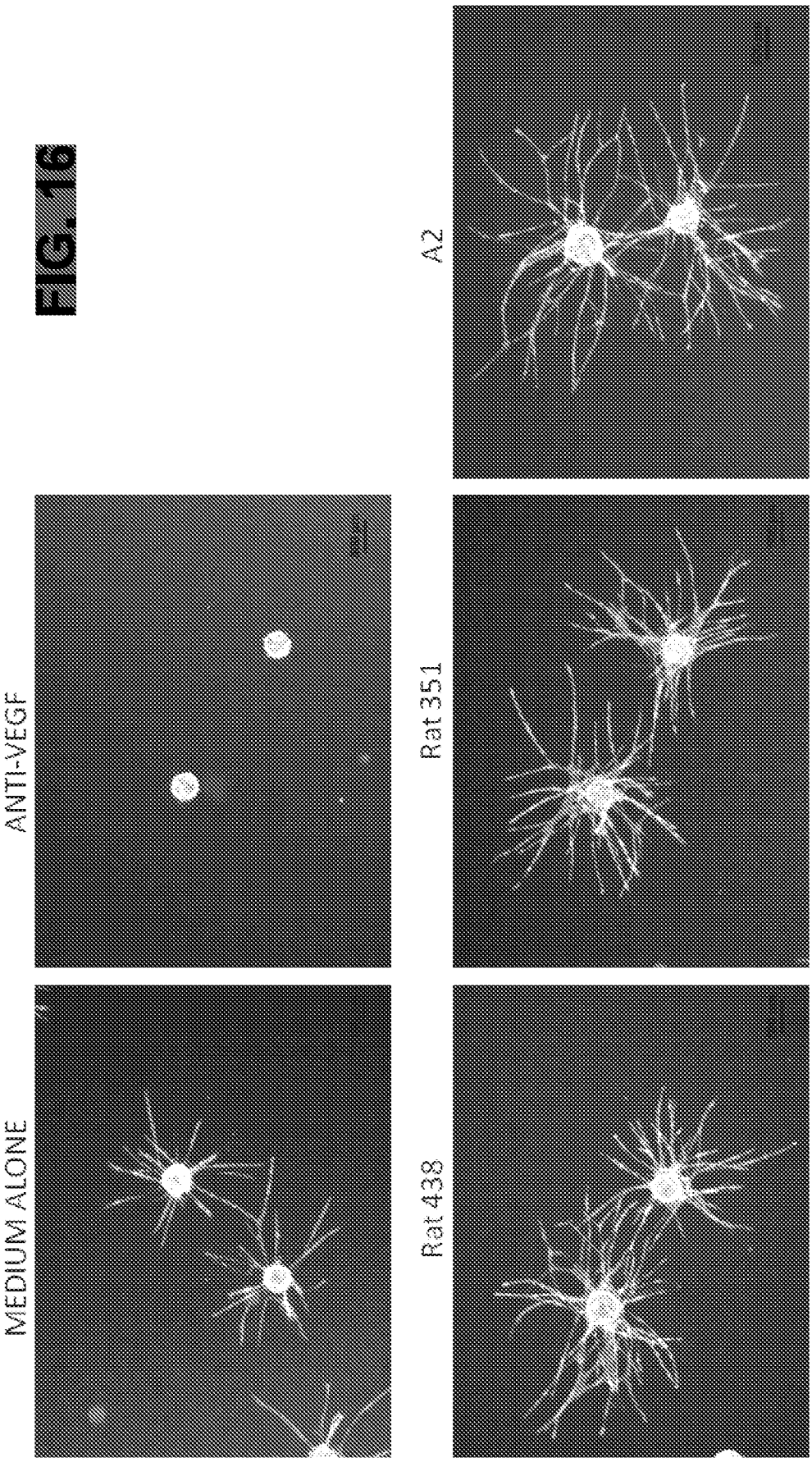
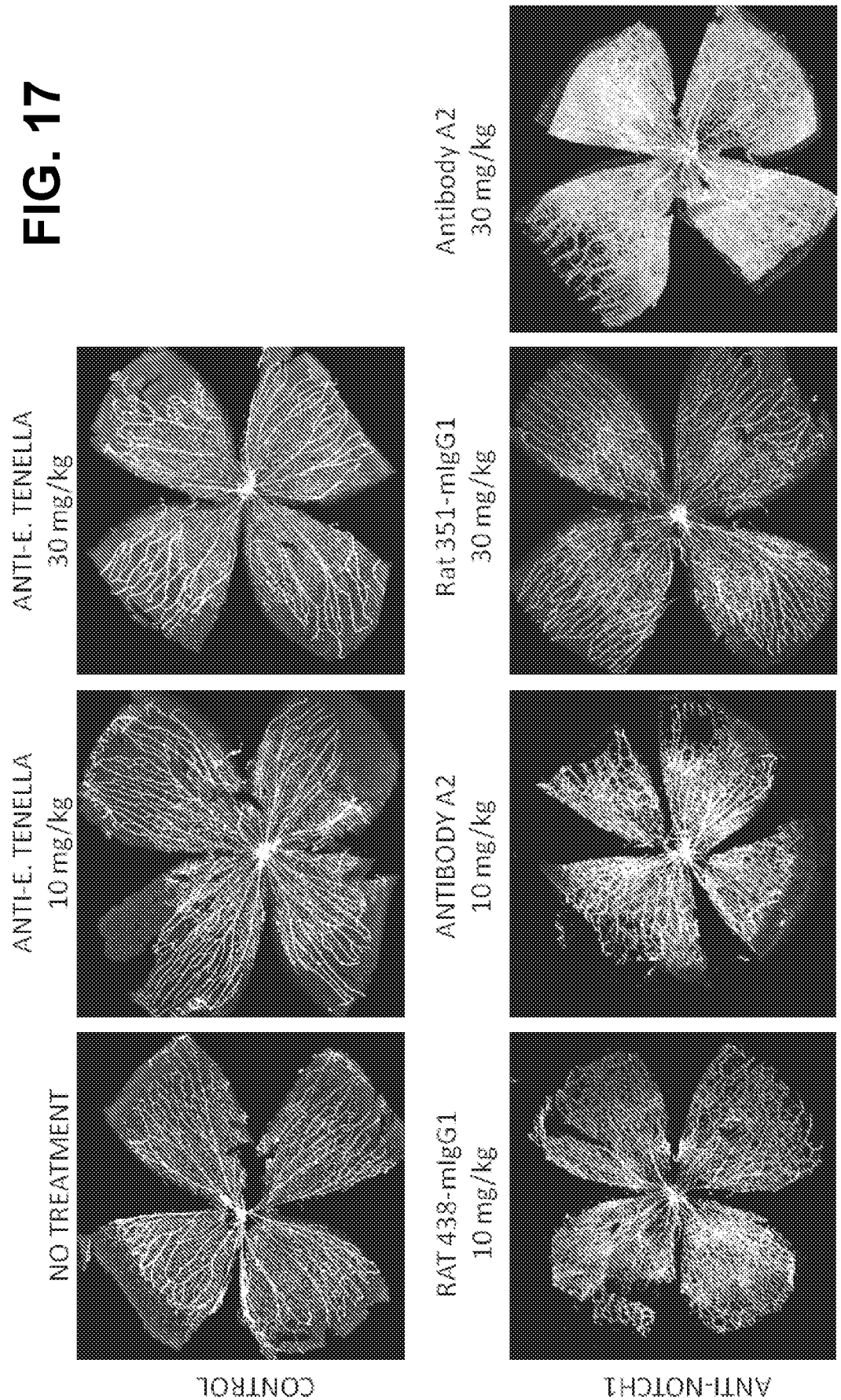


FIG. 16



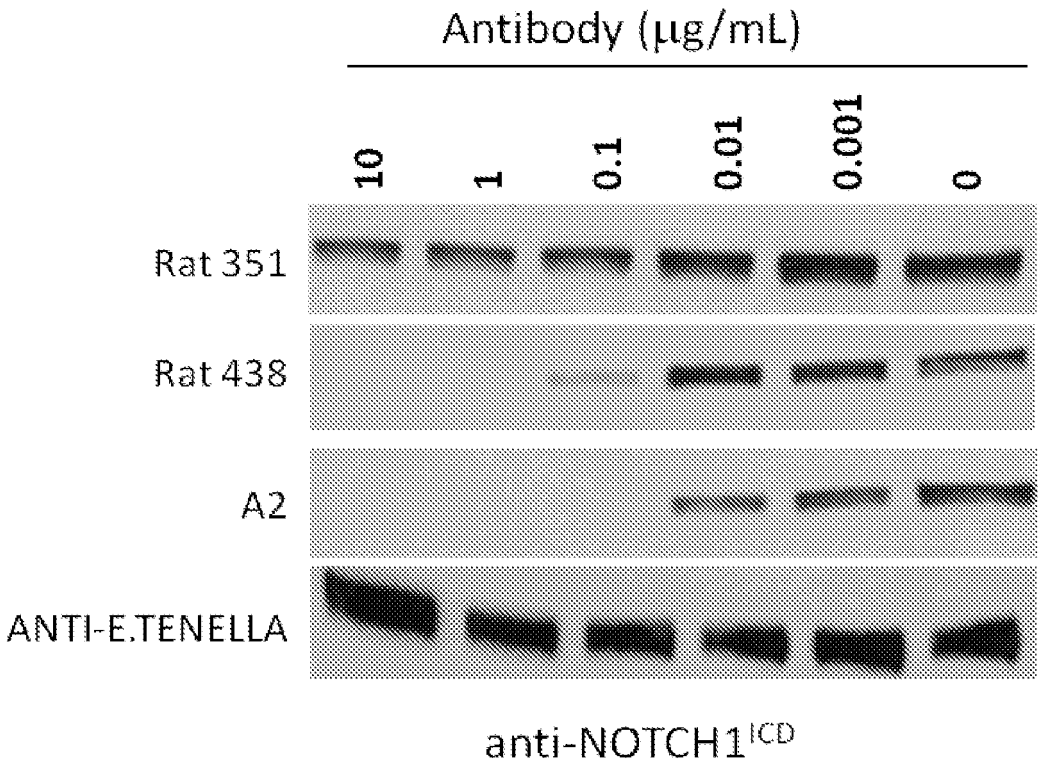
Representative epifluorescent images of CD31-Cy3 immunostaining of in a HUVEC-FGBA using human lung tumor-associated fibroblasts

FIG. 17



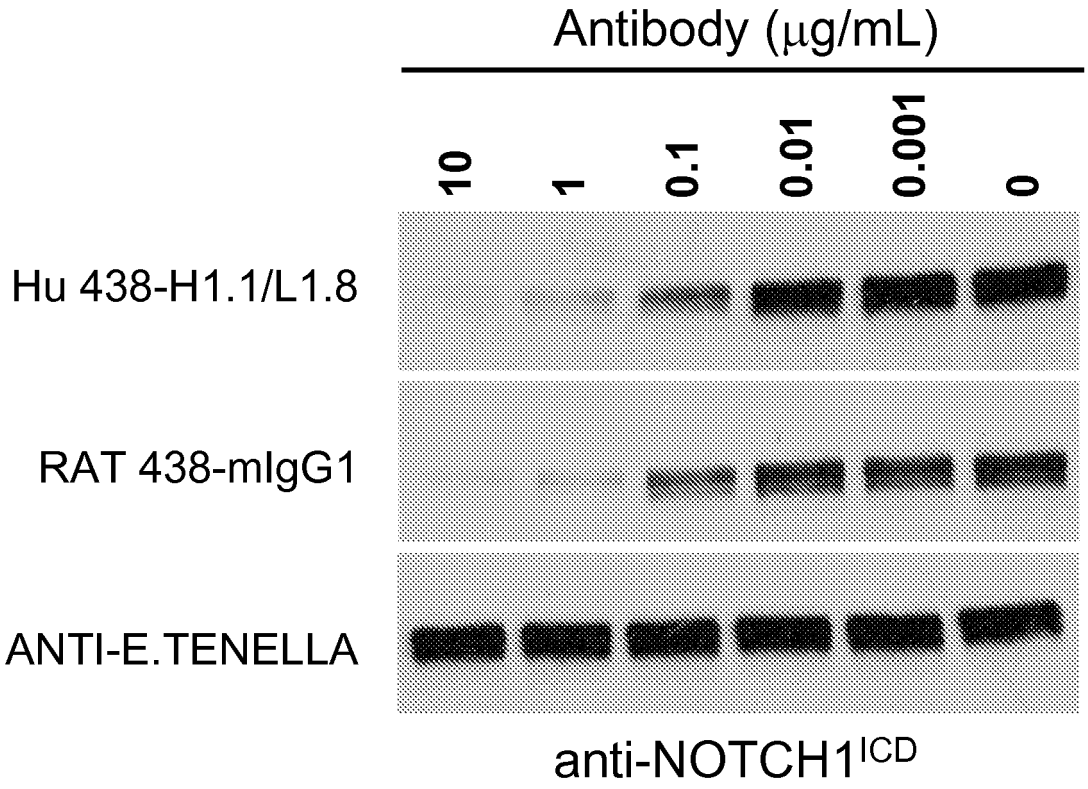
Representative confocal images of Isolectin B4-Alexa488 staining in a mouse retinal model of angiogenesis

FIG. 18



Western blot analysis of protein extracts generated from CCD1076SK human fibroblasts plated on recombinant human DLL4 ligand

FIG. 19



Western blot analysis of protein extracts generated from HPB-ALL cells

FIG. 20

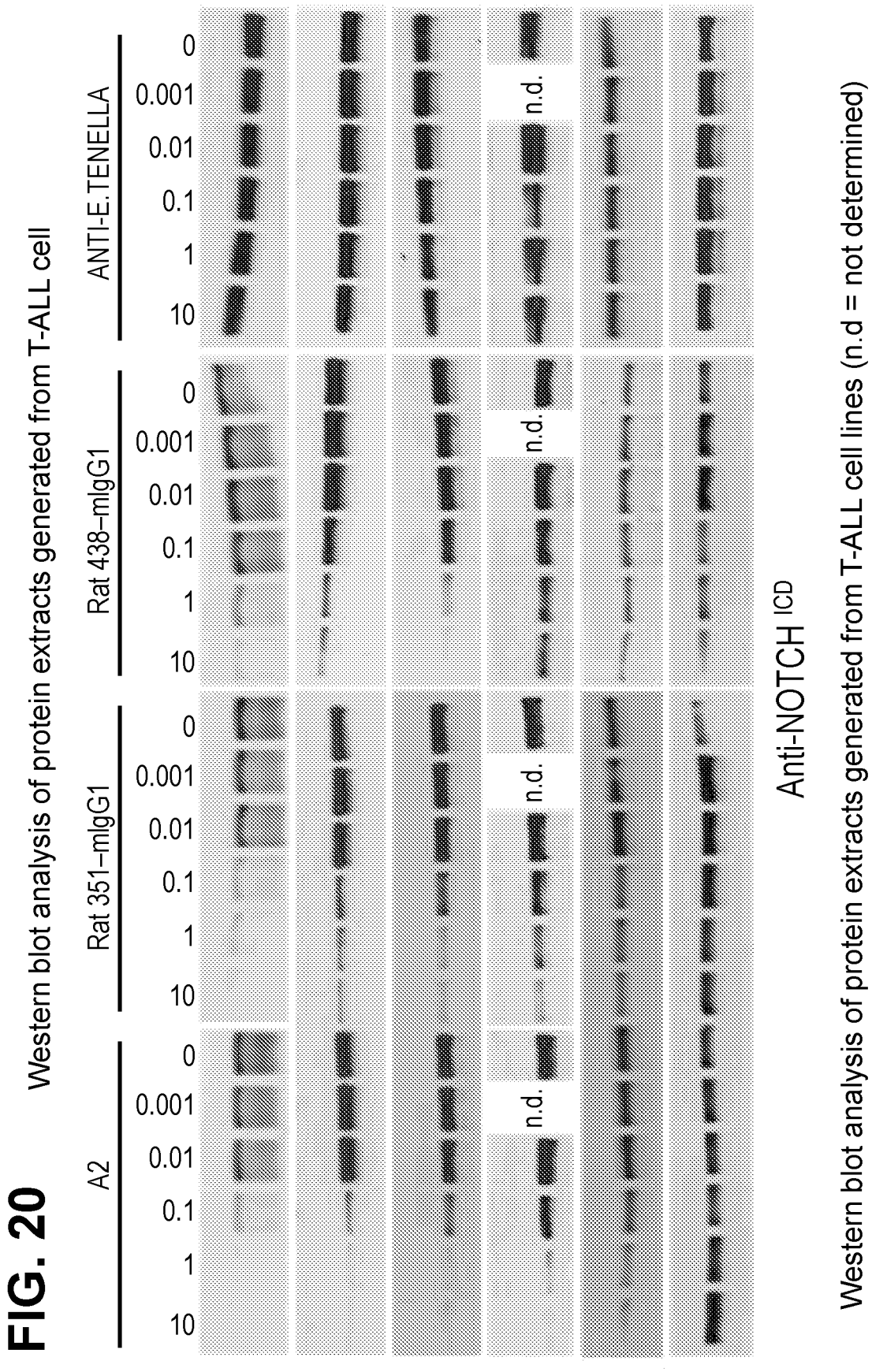

Western blot analysis of protein extracts generated from T-ALL cell
A2
Rat 351–mIgG1
Rat 438–mIgG1
ANTI-E.TENELLA
0
0.001
0.01
0.1
1
10
n.d.
Anti-NOTCH ICD
Western blot analysis of protein extracts generated from T-ALL cell lines (n.d = not determined)

FIG. 21

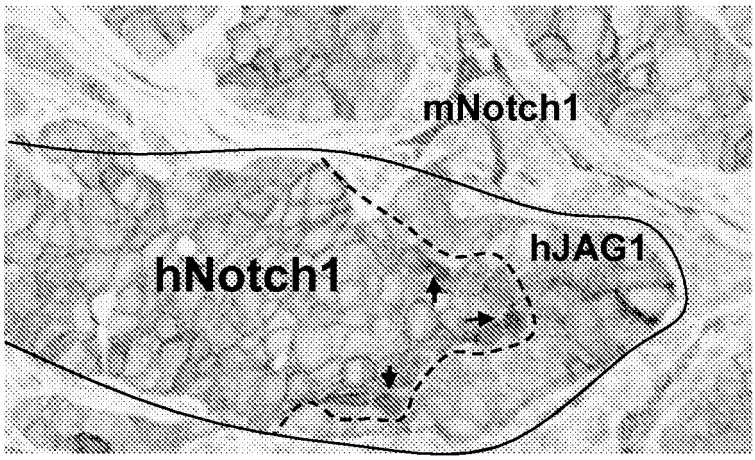


FIG. 22

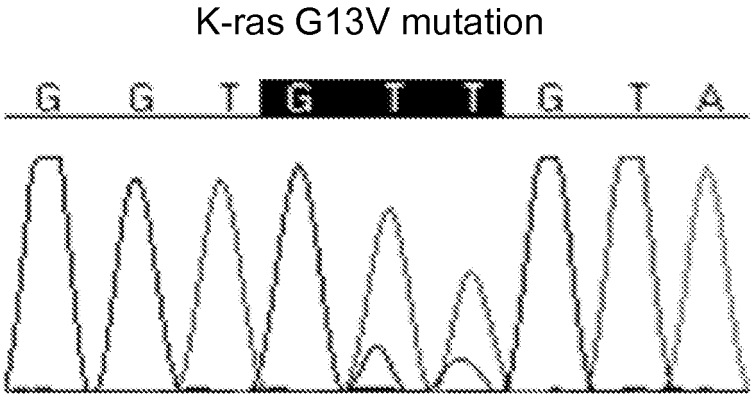
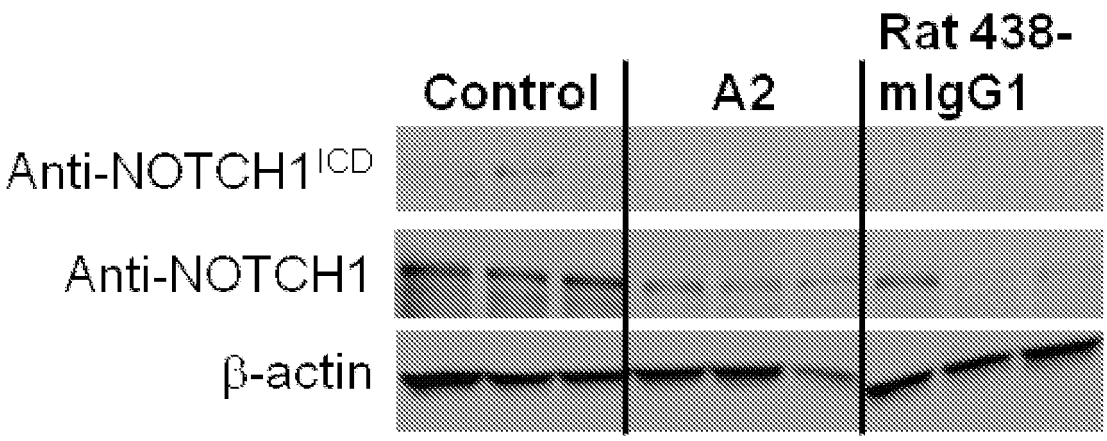
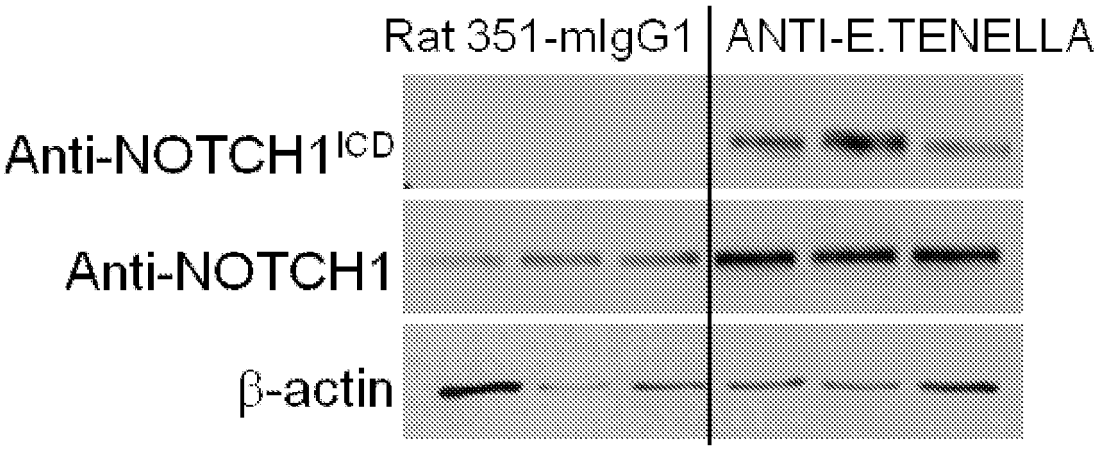


FIG. 23



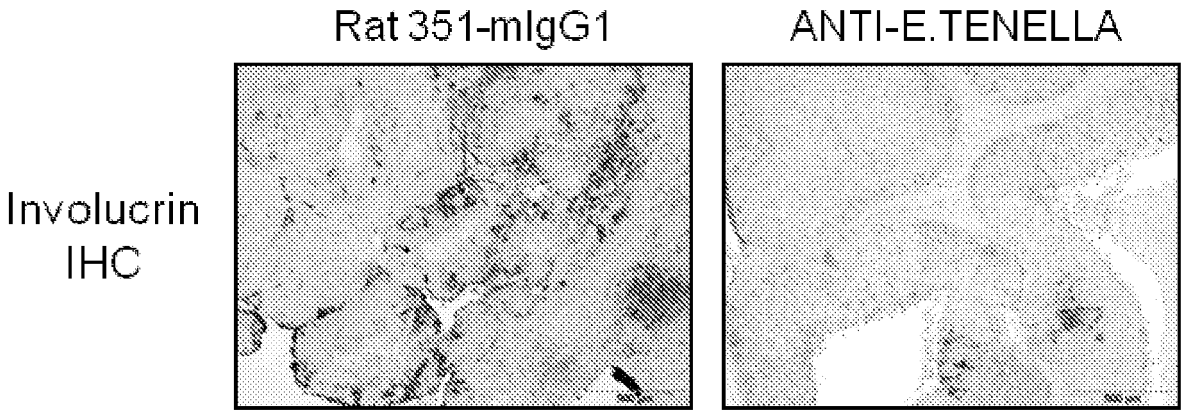
Western blot analysis of protein extracts generated in 37622A1 NSCLC patient derived xenografts

FIG. 24



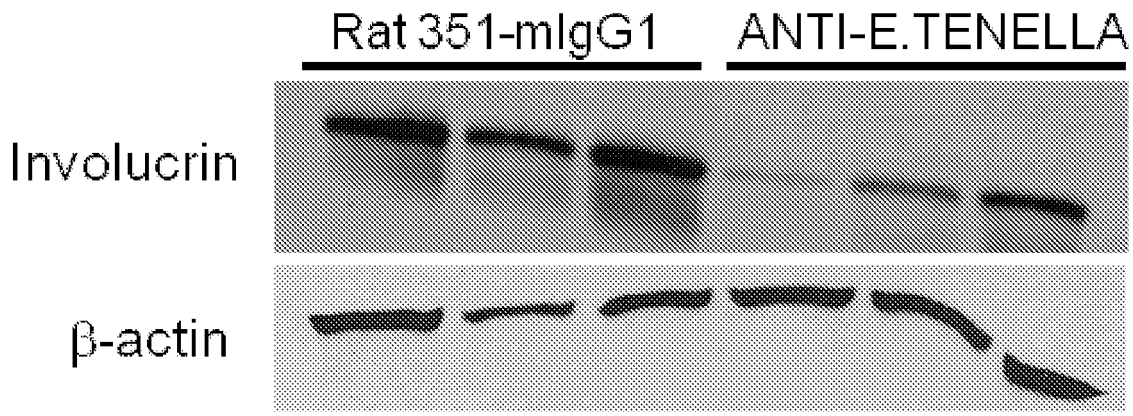
Western blot analysis of protein extracts generated in 87393A1 NSCLC patient derived xenografts

FIG. 25



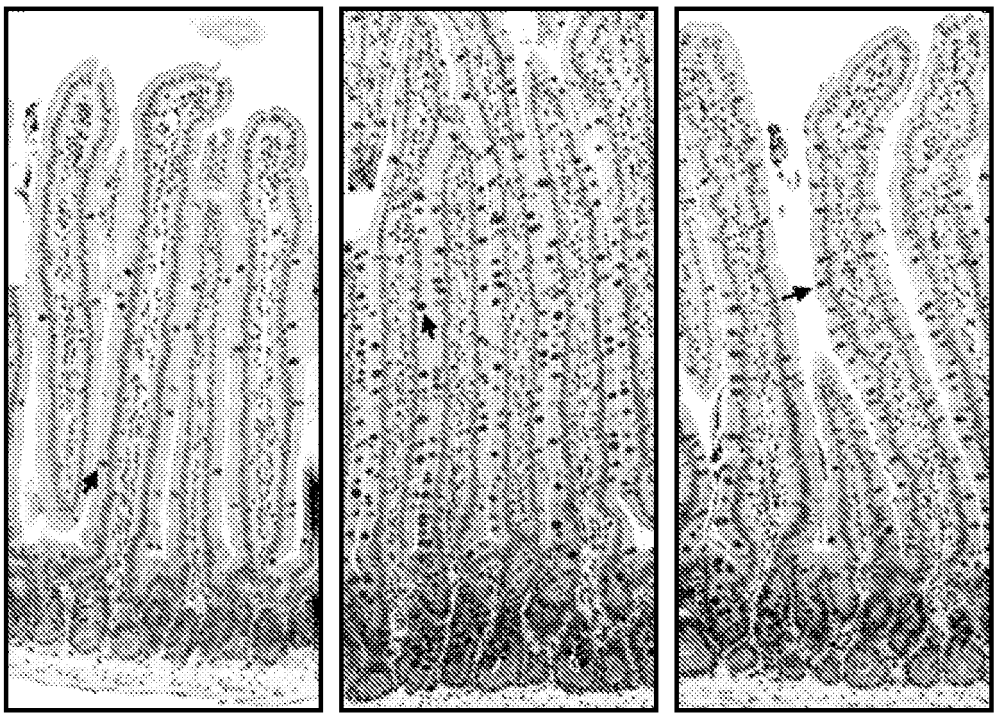
Immunohistochemical detection of involucrin expression in 87393A1 NSCLC patient derived xenografts

FIG. 26



Western blot analysis of involucrin expression in 87393A1 NSCLC patient derived xenografts

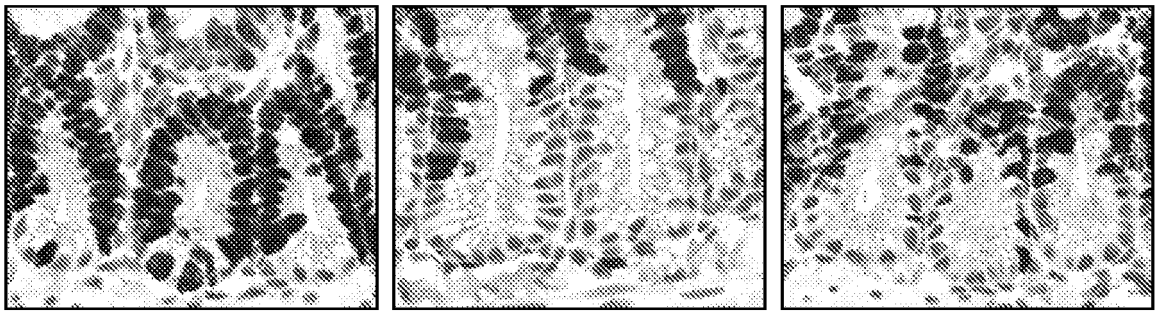
FIG. 27



ANTI-E.TENELLA | Rat 438-mIgG1 | A2

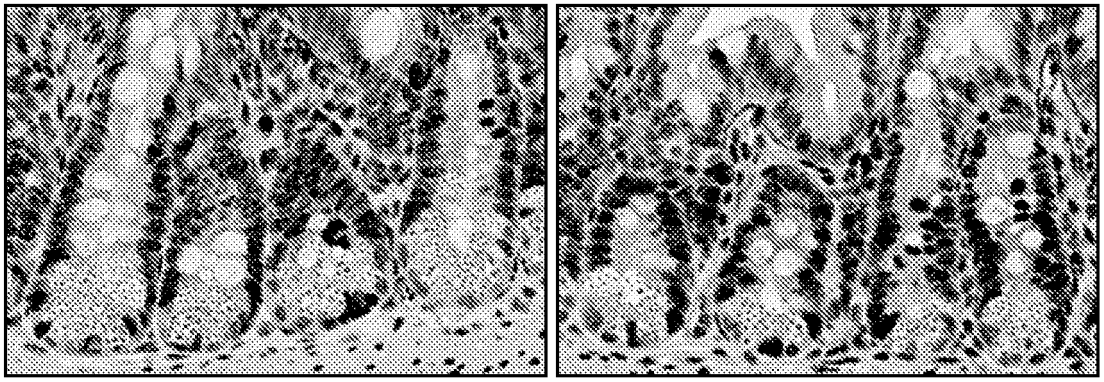
Histochemical identification of secretory goblet cells using Alcian Blue stain on the ileum section of mouse intestines from Calu-6 efficacy study

FIG. 28



Anti-Ki67 immunohistochemistry on mouse intestinal crypts from Calu-6 efficacy study

FIG. 29



Anti-Ki67 immunohistochemistry on mouse intestinal crypts from 87393A1 NSCLC patient derived xenografts efficacy study